# Closed-Loop Control of Weld Pool Depth Using a Thermally Based Depth Estimator

*A thermally based depth estimator provides accurate and fast estimates for real-time control of weld pool depth in gas metal arc welding*

BY J.-B. SONG AND D. E. HARDT

ABSTRACT. Depth of joint penetration is the most important geometric attribute in many welding situations, but no robust method exists for direct measurement of this quantity. In this paper, a method for real-time estimation of the depth of partial penetration welds is proposed based on the solution of an inverse heat transfer problem. A closed-loop control system for weld pool depth using this thermally based depth estimator is also presented. From point temperatures measured on the backside of the workpiece, Gaussian heat source parameters (efficiency and distribution) are identified by solving an inverse 3-D analytical heat conduction problem. The heat source description obtained this way can define the isotherms internal to the weldment and thus the depth of penetration. The estimation algorithm is designed such that the temperature measurement, parameter identification, and estimation of the depth are performed in real-time in order to deal with time-varying welding conditions. A series of experiments performed under a variety of welding conditions indicates that the method can provide depth estimates of acceptable accuracy and speed for real-time control. The estimator has also been successfully implemented in a series of closed-loop control experiments to regulate the depth. The depth estimator and control system are developed here for gas metal arc butt joint welds with finger penetration, but these can be extended to other arc welding processes and geometries.

*J.-B. SONG is an Assistant Professor, Department of Mechanical Engineering, Korea University, Seoul, Korea. D. E. HARDT is a Professor of Mechanical Engineering, Laboratory for Manufacturing and Productivity, Massachusetts Institute of Technology, Cambridge, Mass.*

## Introduction

Weld quality features such as final metallurgy and joint mechanics are not measurable on-line for control; thus, some indirect way of controlling the weld quality is necessary. A comprehensive approach to in-process control of welding includes both geometric features of the bead (such as bead width, depth and height) and thermal characteristics (such as heat-affected zone and cooling rate). Figure 1 shows a typical weld cross-section observed in gas metal arc welding (GMAW). The geometric features can be related to the basic mechanics of the joint, and the thermal features can indicate the final microstructure of the material.

**KEY WORDS**

Closed-Loop Control
Weld Pool Depth
Depth Estimator
Thermal-Based
Real-Time Control
GMAW
Inverse Heat Transfer
Heat Transfer Model
Depth Sensor
Bead-on-Plate Welds

The key geometric attribute of a major class of welds is the depth of penetration since it is a direct indicator of weld strength or side wall fusion. However, direct measurement of this quantity is quite difficult since the depth is not directly visible and the pool boundary is a very hot solid-liquid interface. Several investigators (Refs. 1, 2) have demonstrated the use of ultrasonic reflection to detect this solid-liquid interface, but this technique is not very accurate because of the problem of diffusion of the signal and the distortion caused by steep temperature gradients. Attempts have been made to indirectly estimate the depth based on surface vibrations of the weld pool (Refs. 3–5), but it has been shown by Zacksenhouse and Hardt (Ref. 6) that surface waves can only be correlated to bulk fluid oscillation for full penetration welds. Other research has been directed toward experimentally correlating the depth of penetration to surface variables that can be measured during welding. These include visible geometric features, which can be measured by video techniques (Ref. 7), or thermal features, which can be sensed using infrared thermography (Ref. 8). Specifically for penetration, surface radiation was used to directly regulate depth by Nomura, *et al.* (Ref. 9). Using the radiation from underneath the weld, the torch current was modulated to maintain a constant radiation level. This was correlated to the depth, but was easily corrupted by plate thickness or preheat changes, and gave no detail on the actual pool shape.

The first attempt at direct depth estimation using surface temperature profiles was made by Bates and Hardt (Ref.

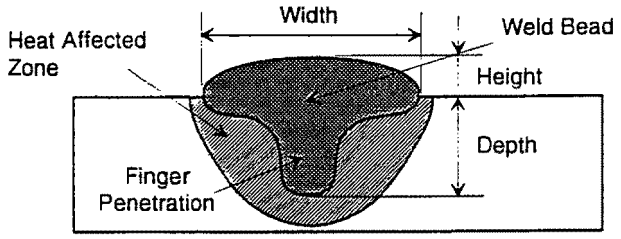


*Fig. 1 —Typical weld cross-section for gas metal arc welding.*

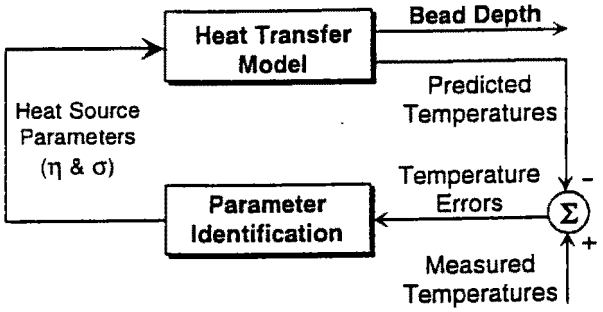


*Fig. 2 — Block diagram of a thermally based depth estimator.*

10). In this method, a single-source pure conduction model of welding was "tuned" to match measured temperature gradients by varying a pair of unknown heat source parameters. Limited experimental work (Ref. 11) demonstrated that although the basic method had promise, the method of application was flawed. In addition, it was applied only to gas tungsten arc welding, which creates rather simple pool geometries.

Therefore, a more robust method is necessary to measure or estimate the depth of penetration produced by GMAW for in-process control. Since the heat conduction solution with ordinary heat sources, such as a point heat source (Ref. 12) or a Gaussian heat source (Ref. 13), cannot successfully describe the "finger penetration" observed in GMAW (Fig. 1), some modification of the heat source is necessary. In addition, the algorithm is designed to deal with time-varying welding conditions for in-process control. The general procedure of this algorithm is shown in Fig. 2. By comparing predicted backside point temperatures with measured values, a prediction error is computed. This error is then used to drive a nonlinear parameter identification scheme. The heat source parameters obtained this way can define the isotherms internal to the weldment. The pool shape (including the depth) is then found by seeking the isotherm corresponding to the melting temperature of the material.

## Derivation of Temperature Expression

The dominant form of heat transfer in welding is conduction through the weldment from the solid-liquid interface. Within the pool, most heat transfer is by vigorous convection, and the relationship between the heat source and the pool shape is quite complex. However, Rosenthal (Ref. 12) showed that a pure conduction solution associated with a simple point heat source could effectively predict far-field temperature distribution in the solid. Unfortunately, this conduction solution yielded only circular isotherms and thus circular pool profile since a point heat source was used in the formulation.

In an attempt to produce more realistic weld pool profiles, Eagar and Tsai (Ref. 13) modeled the arc as a Gaussian distributed heat source, which can be expressed as

$$q(x,y)=\frac{\eta Q}{2\pi\sigma^2}exp\left(-\frac{x^2+y^2}{2\sigma^2}\right) \quad (1)$$

where $\eta$ and Q are the efficiency and total heat input, and $\sigma$ is the distribution parameter that corresponds to the standard deviation of a Gaussian function. The temperature at a point (x, y, z) at time t was derived based on this Gaussian heat source model (Ref. 13) as follows:

$$T(x,y,z,t)-T_0=$$
$$\int_0^t \frac{\eta Q}{\pi\rho c}\frac{(16\pi\alpha\tau)^{-1/2}}{2\alpha\tau+\sigma^2}$$
$$exp\left(-\frac{(x+v\tau)^2+y^2}{4\alpha\tau+2\sigma^2}-\frac{z^2}{4\alpha\tau}\right)d\tau \quad (2)$$

where $T_0$ is the initial temperature of the material, $\rho$, c and $\alpha$ (=k/$\rho$c) are the density, specific heat, and thermal diffusivity of the material, respectively. The heat source is attached to moving coordinates O-xyz (the moving origin, O, is on the surface underneath the welding arc and moving with the torch along the positive x-axis, which lies in the direction of welding, and the y-axis is placed in the transverse direction, and z-axis is placed in the transverse and thickness of the plate, downward. Note that Equation 1 was derived on the assumptions that the material properties (*e.g.*, $\rho$, c and $\alpha$) are independent of the temperature. This assumption will cause some errors when temperatures and gradients are high, but since the model output of concern is in the far field (*i.e.*, on the weldment surface) the effect of this assumption is minimal. Since the coordinates (x, y, z) are measured relative to the moving source, the temperature distribution referenced to this moving coordinate system reaches the so-called quasi-stationary (or steady) state as time approaches infinity.

With the combination of two adjustable parameters, efficiency ($\eta$) and distribution ($\sigma$), this model could predict more realistic weld pool shape and size as shown in Fig. 3. As the distribution parameter increases from zero to some value, the width of the pool grows while the depth decreases, since the heat input from the arc is spread over more area as the distribution becomes larger. Therefore, for any value of the distribution, the half width of the pool is larger than the depth. However, many welding processes produce more complex weld pool shapes (*e.g.*, GMAW pool shown in Fig. 1). In an attempt to deal with this more complex pool shape, Song and Hardt (Ref. 14) and Doumanidis (Ref. 15) proposed a new model where dual Gaussian heat sources were applied instead of a single Gaussian heat source. The weld pool shape shown in Fig. 4 can be broken into two parts: 1) a horizontal portion caused primarily by the top Gaussian heat source; and 2) a vertical portion (*i.e.*, finger penetration) caused by the lateral Gaussian heat source. The overall temperature distribution and pool shape can be found by superposition of the two temperature distributions of the dual heat sources. Four adjustable parameters ($\eta_1$, $\sigma_1$, $\eta_2$, and $\sigma_2$) can now be used in describing the complex weld pool profiles, thus providing greater flexibility compared to either the point source with only one parameter or the single Gaussian source model with two parameters. In the dual source model, the lateral heat source was introduced to account for the finger penetration observed in GMAW, which is mainly due to the transfer of high temperature metal driven by the droplet momentum. Therefore, the formation of the finger penetration cannot be described simply by a lateral Gaussian heat source from a physical point

of view. However, the use of the lateral Gaussian heat source (and thus the dual heat sources) can be justified for the following two reasons. First, whatever mechanisms form the weld pool shape, only heat conduction is involved in the solid outside of the molten pool. The liquid-solid interface that corresponds to the weld pool shape plays an important role in specifying the boundary conditions. Therefore, a reasonable description of the weld pool shape using the dual Gaussian heat source model is important in predicting the temperature distribution in the solid, especially in the near-field around the finger penetration. Second, this dual source model will be used to solve an inverse heat transfer problem. In most research involving the prediction of the weld pool shape and size, the efficiency and/or the distribution of a heat source are first found either empirically or analytically. The pool shape and temperature distribution are then sought using those parameters obtained before. However, in the inverse heat transfer approach, the temperature distribution is measured first in the form of the surface temperatures at various points and then the parameters that predict such a temperature distribution are computed. Therefore, the parameters, such as efficiency and distribution, do not have to be measured directly. This inverse approach enables the dual heat source (which does not physically exist) to be used in the formulation.

The dual heat source model can adequately describe the entire weld pool contour; however, estimating the depth of penetration rather than predicting the entire weld pool shape is of more interest here. Recall that the top Gaussian heat source mainly accounts for the width portion of the weld pool, whereas the lateral one for the depth portion or finger. Even though the overall melting isotherm results from both heat sources, the long diffusion paths suggest that the penetration isotherms will mainly be related to the lateral heat source for moderately thick material. Accordingly, the top source can be eliminated for the depth estimator implementation as shown in Fig. 5. This simplification is valuable in terms of computation burden and the robust convergence of the depth estimation algorithm. Also, it was shown experimentally that ignoring the top source contribution had little effect on the accuracy of penetration prediction. In addition, the temperature measurement on the top side are often difficult because of the arc light (a detailed explanation and performance of the dual source model can be found in Ref. 16).

Since the lateral Gaussian source model can adequately predict the depth of penetration, only this model will be considered from this point on. The temperature expression based on the lateral Gaussian heat source can be easily obtained by exchanging y and z coordinates in Equation 2 as follows:

$$T(x,y,z,t) - T_0 = \int_0^t \frac{\eta Q}{\pi\rho c} \frac{(16\pi\alpha\tau)^{-1/2}}{2\alpha\tau + \sigma^2} exp\left( -\frac{(x+v\tau)^2 + z^2}{4\alpha\tau + 2\sigma^2} - \frac{y^2}{4\alpha\tau} \right) d\tau \quad (3)$$

A serious limitation of all the above models is that they were all derived under the assumption that all the welding conditions, such as the efficiency, heat input, and travel speed were kept constant during the process, whereas welding conditions often change during the process. In addition, if feedback control is to be used, the welding variables that are the control inputs are constantly changing to meet the specified requirements. As a result, the algorithm must have the ability to cope with time-varying welding conditions.

To deal with this problem, the time integral in Equation 3 is divided into many small time intervals. In control implementation, the control inputs, which are the welding conditions in this case (*i.e.*, travel speed and wire feed rate in GMAW), cannot vary continuously, but can change only at the sampling instants. It is assumed, therefore, that welding conditions are kept constant during each sampling interval, and can change at each sampling instant. With this assumption, a temperature expression can be derived for varying welding conditions. In Equation 3, when a point (x,y,z) and time t at which the temperature is desired are known, the temperature is computed by once integrating over that time period from $\tau = 0$ to t since all the variables in the integrand are constant. However, in the time-varying case, the contributions of the time intervals 1 through k to the temperature rise at the point of interest must be computed when we are interested in the temperature at a point (x,y,z) at time $t = kT_s$, which is the integer multiple of the sampling period Ts. Figure 6 illustrates the efficiency, travel speed, and x position of the heat source for each time interval. It is noted that the heat input Q is assumed to be constant for all time intervals because the arc efficiency ($\eta$), which always appears together with the heat input Q, is able to reflect the change of the heat input. The position of the heat source in the x-direction at time $\tau$ at each interval can be expressed as

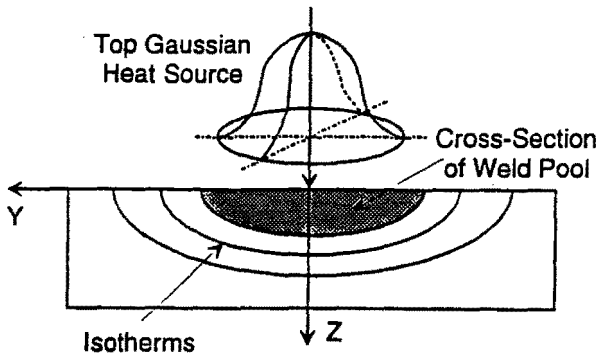


*Fig. 3 — Weld pool shape and isotherms in a top Gaussian heat source model. Note that the half-width is larger than the depth.*

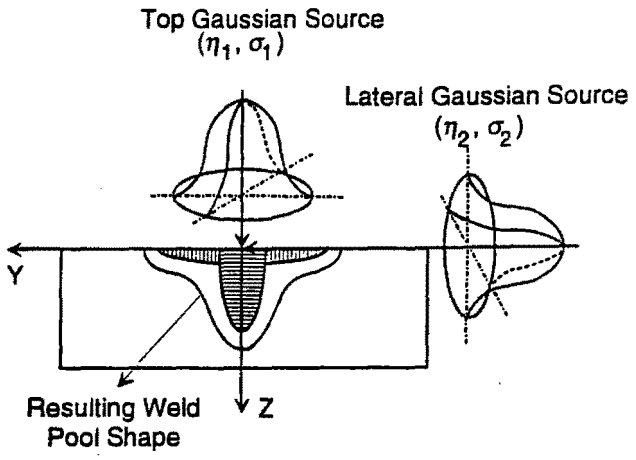


*Fig. 4 — Weld pool shape and isotherms in a dual Gaussian heat source model.*

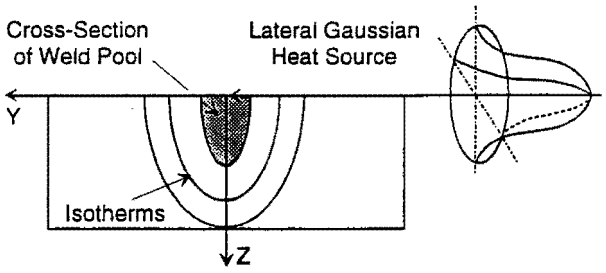


*Fig. 5 — Weld pool shape and isotherms in a lateral Gaussian heat source model. Note that the depth is larger than the half-width.*

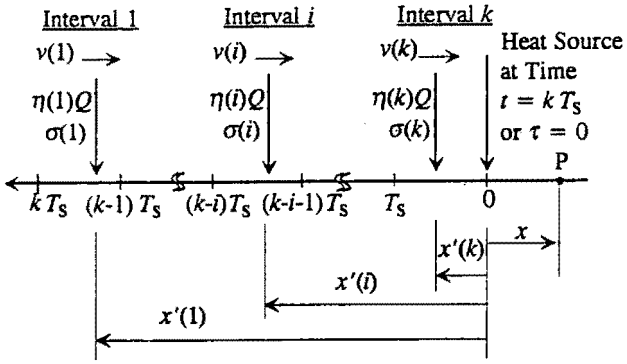


*Fig. 6 — Welding conditions and heat source positions for each time interval.*

$$x'(k) = v(k)\tau$$
$$x'(k-1) = v(k)T_s + v(k-1)(\tau - T_s)$$
$$\vdots$$
$$x'(i) = \left(\sum_{j=i+1}^{k} v(j)\right)T_s + v(i)$$
$$\{\tau - (k-i)T_s\} \quad (i \le k-1) \tag{4}$$

With the notations defined in Fig. 6, the temperature at a point (x,y,z) at time t = kTs becomes

$$T(x,y,z,kT_s) - T_0 = \sum_{i=k}^{1}\left[\int_{(k-i)T_s}^{(k-i+1)T_s}\left\{\frac{\eta(i)Q}{\pi\rho c}\frac{(4\pi\alpha\tau)^{-1/2}}{2\alpha\tau+\sigma(i)^2}\sum_{n=-\infty}^{\infty}\exp\left(-\frac{(x+x'(i))^2+(z+2nh)^2}{4\alpha\tau+2\alpha(i)^2}\right)\exp\left(-\frac{y^2}{4\alpha\tau}\right)\right\}d\tau\right] \tag{5}$$

where x'(i) is given by Equation 4 and h is the thickness of the plate. The second summation has been introduced to implement the method of images which is used to account for finite thickness of the plate (Refs. 12, 17). In actual computation, only two sources, one just above the top surface and the other just below the bottom surface, are sufficient for moderately thick material. Note that the integrand of the first summation represents the contribution of the interval i to the temperature T(x, y, z, $kT_s$). Even though the above temperature expression shows that temperature at time t = $kT_s$ is composed of contributions from the time intervals up to k, the contributions from the intervals well before k are almost negligible. Thus, only a few time intervals are actually included to compute the temperature, and the number of intervals required depends strongly on the travel speed. This can be explained as follows:

Temperatures around the heat source are determined by both the direct heat input from the heat source at that instant and the heat conducted away from the molten or solidified pool behind the measurement points caused by the past heat input. However, as the heat source moves faster, the travel speed exceeds the heat diffusion speed, which means that these temperatures are determined mainly by the heat input from the heat source around that time. Therefore, as the travel speed increases, fewer intervals are required. As a result of these observations, the above temperature expression can be implemented with only a moderate amount of computation.

## Parameter Identification Scheme

No direct solutions for the parameters (η, σ) are available because the temperature expression in Equation 5 depends nonlinearly on the parameters to be identified. Hence, an iteration-based method must be adopted in which convergence and computation time become critical. Accordingly, a nonlinear least-square problem is formed where a least-squares objective function E is defined as

$$E = \sum_{n=1}^{N}\left(T_n^* - T_n\right)^2 \tag{6}$$

where $T_n^*$ and $T_n$ represent the measured temperature and the temperature predicted from Equation 5 at the measurement point n, respectively, and N is the number of the measurements. The best values for (η, σ) are then obtained when the objective function is minimized. There are several ways to minimize the objective functions but the so-called Marquardt algorithm is most commonly used (Ref. 18). This algorithm is composed of two different algorithms, Gauss-Newton method and Steepest Descent method. With a combination of these two algorithms, the Marquardt algorithm can be expressed as

$$\left(P^T P + \lambda I\right)\delta q = P^T\left(T^* - T\right) \tag{7}$$

where P is the Jacobian matrix (N by 2) whose elements are the derivatives of the objective function with respect to the parameters (η and σ), I is the identity matrix, and δq is the vector whose elements are the incremental corrections to the solutions of each iteration. Note that λ is a factor adjusting the degree of participation of each method each iteration. The Gauss-Newton method converges rapidly when good initial estimates of the unknown parameters are available. However, the iteration tends to diverge if the initial estimates are not close enough to the correct solutions. On the contrary, the steepest descent method converges for poor initial guesses, but do so very slowly. The combination proves to give both fast and robust convergence for reasonably chosen initial guesses.

The Marquardt algorithm can be easily applied to the parameter identification of the heat source parameters. In this case, the Jacobian matrix becomes

$$P = \begin{bmatrix} \dfrac{\partial T_1}{\partial \eta(k)} & \dfrac{\partial T_1}{\partial \sigma(k)} \\ \vdots & \vdots \\ \dfrac{\partial T_N}{\partial \eta(k)} & \dfrac{\partial T_N}{\partial \sigma(k)} \end{bmatrix} \tag{8}$$

and Equation 7 can be expressed as

$$\begin{bmatrix} \sum_{n=1}^{N}\left(\frac{\partial T_n}{\partial \eta(k)}\right)^2 + \lambda & \sum_{n=1}^{N}\left(\frac{\partial T_n}{\partial \eta(k)}\frac{\partial T_n}{\partial \sigma(k)}\right) \\ \sum_{n=1}^{N}\left(\frac{\partial T_n}{\partial \eta(k)}\frac{\partial T_n}{\partial \sigma(k)}\right) & \sum_{n=1}^{N}\left(\frac{\partial T_n}{\partial \sigma(k)}\right)^2 + \lambda \end{bmatrix}\begin{Bmatrix} \delta\eta(k) \\ \delta\sigma(k) \end{Bmatrix} = \begin{Bmatrix} \sum_{n=1}^{N}\frac{\partial T_n}{\partial \eta(k)}\left(T_n^* - T_n\right) \\ \sum_{n=1}^{N}\frac{\partial T_n}{\partial \sigma(k)}\left(T_n^* - T_n\right) \end{Bmatrix} \tag{9}$$

The general rule is that λ is initially chosen as a rather large value to assure the convergence (typically, λ = 0.01), and then continuously decreased (*e.g.*,

a factor of 10 each iteration) as the minimum of the objective function is approached. However, if the iteration starts diverging during computation, $\lambda$ is increased. As the minimum is approached, only the Gauss-Newton method has an important role since $\lambda$ approaches zero.

Since the welding conditions are varying, this iteration process is done every sampling interval in order to find new heat source parameters of each interval. Simulations show that this algorithm is robust and fast enough to identify the parameters for in-process control purposes.

## Experiments: Depth Estimator

To examine performance of the algorithm, a series of welding experiments was conducted using GMAW. The experimental setup is shown schematically in Fig. 7. The workpiece moves in the direction opposite to the welding direction, while the torch and temperature measurement system remain stationary. The wire feed rate and the travel speed are used as the process inputs.

The algorithm for the depth estimator is based on the assumption that accurate temperature measurements at the specified points are available in real-time. In an effort to meet this requirement, a temperature-measurement system has been designed and built (Ref. 19). This system is based on total radiation pyrometry technique where surface temperatures are measured by collecting the emitted thermal radiation from points of interest at all wavelengths in the infrared (IR) spectrum. Figure 8 illustrates a schematic of the temperature-measurement systems.

A thermopile detector is used in the measurement system because it is sensitive to a broad wavelength range in the IR spectrum and the supporting electronic circuits are simple. As an optical guide for the IR radiation from the workpiece to the detector array, spherical concave and plane mirrors are used. Three or four point temperatures were measured around the torch position on the backside of the workpiece each sampling time. The above temperature-measurement system is shown to provide accurate and fast temperature data (5 Hz) to the depth estimator algorithm.

The experiments were conducted based on a bead-on-plate welding. The primary metals were low-carbon steels which are 6.35 mm (¼ in.) thick. The topside of the workpiece was ground to remove oxides, while the backside was cleaned chemically in order to improve temperature measurements. An Ar + 2% oxygen gas mixture was used as a shielding gas for this experiment. At the sampling frequency of 2 Hz, three or four point temperatures on the backside of the weldment were measured and fed to the PC, which executed the depth estimation algorithm. After welding, the weldment was sectioned, polished and etched to reveal the cast metal zone, and the actual weld profile.

Material properties such as density, specific heat and thermal diffusivity change as a function of temperature. As shown in Equation 3, the density and specific heat can be accounted for by adjustment of the efficiency, but the thermal diffusivity is entangled with other factors. An average value of 0.08 $cm^2/s$ was taken for the mild steel and showed good agreement in estimation.

Measurement locations are particularly important to the performance of the real-time depth estimator. There are some limitations to the selection of the measurement points for the depth estimation. The first reason is related to the characteristics of the transient form of the depth estimation algorithm. The heat source parameters $\eta(k)$ and $\sigma(k)$ at time interval k are identified based on how changes in these parameters affect predicted temperatures to match the measured ones at time $t = kT_s$. If the measurement points are at the locations covered by the previous intervals (*e.g.*, interval k-1), then the temperatures at these points are not greatly affected by the current heat source parameters for the following reason: the points far from the heat source respond slowly when compared to those around the heat source and these slow responses cannot be effectively used due to the limited sampling period. Thus, correct parameters for the current interval k cannot be identified from those measurements. The space interval covered by the corresponding time interval depends on both the travel speed and the sampling period. The distance covered by the time interval k is then simply $v(k)^* T_s$. Since the sampling period is 0.5 s and the travel speed ranges from 5 to 9 mm/s in the control implementation, the distance ranges from the 2.5 to 4.5 mm accordingly. Figure 9 shows the actual measurement locations that are determined based on the above observations.

To examine the robustness of the estimator to various welding conditions, a comprehensive series of experiments were performed. The experiments were conducted in two stages: 1) constant welding conditions; and 2) time-varying welding conditions. In the first set of experiments, welding conditions were kept constant in each experiment, but various combinations of wire feed rate and travel speed were conducted: travel speed ranging from 5 to 10 mm/s (11.8 to 23.6 in./min) and feed rate ranging from 15 to 30 cm/s (350 to 700 in./min). The experimental results are shown in Fig. 10. In this plot, the abscissa is chosen as the ratios of the wire feed rate to

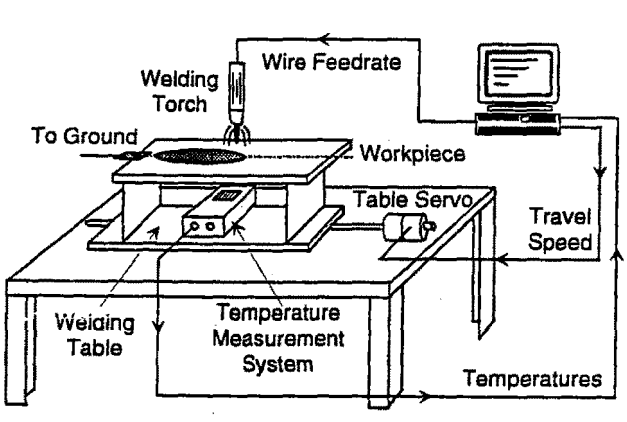


*Fig. 7 — Experimental setup for GMAW.*

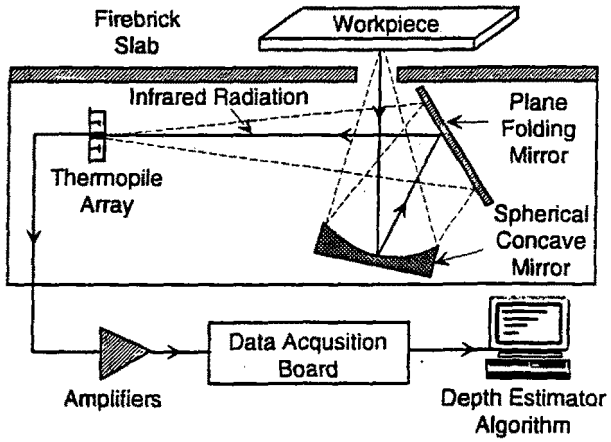


*Fig. 8 — Schematic of temperature measurement system.*

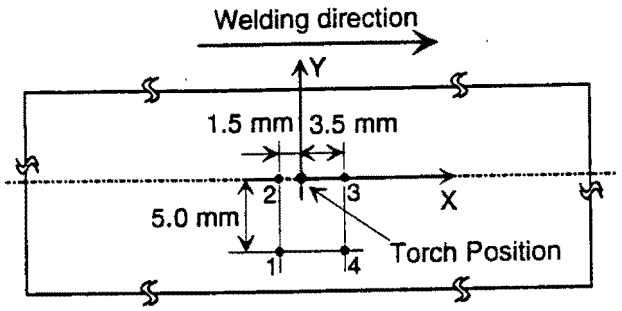


*Fig. 9 — Bottom side temperature measurement locations for depth estimator.*

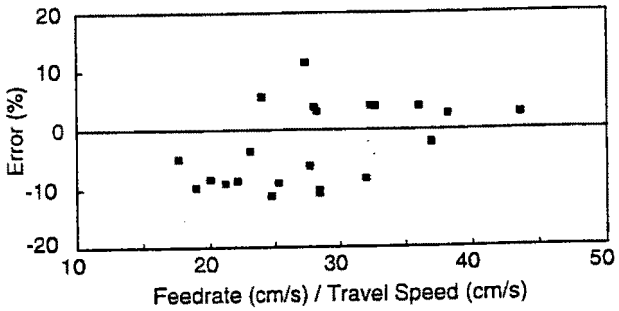


*Fig. 10 — Depth estimation errors for various constant welding conditions (feed rate = 16 to 27 cm/s (378 to 638 in./min), travel speed = 5.0 to 8.5 mm/s (11.8 to 20.1 in./min)).*

the travel speed, which is proportional to the heat input per unit length for the weld. Errors on the depth estimation were bounded by about ±12%.

In the second set of experiments, both the feed rate and travel speed were changed during the process as shown in Fig. 11A. The heat input per unit length for the weld, which is proportional to the ratio of the feed rate (f) to travel speed (v), f/v, is again used as a convenient measure. The heat source parameters and depth were estimated at each sampling interval, and Fig. 11B illustrates the changes in these parameters depending on welding conditions. As expected, the efficiency increases as f/v increases. However, the relation between the distribution and f/v cannot be explained clearly from a physical point of view even though it shows some tendency. It is noted that the values of $\eta$ and $\sigma$ do not represent the physical efficiency and distribution of the welding arc. The weldment was sectioned longitudinally along the welding direction, polished, and etched to reveal the depth variation. This actual depth was compared with the estimated depth by the depth estimator. Figure 11C illustrates this comparison. It is observed that the depth estimate quickly follows the actual changes in the depth. Certain discrepancies in the steady-state responses seemed to be due to the measurement errors because it was difficult to accurately section the weldment along the centerline.

## Closed-Loop Control of Weld Pool Depth

Weld pool depth control systems have not been fully developed because the depth cannot be directly measured. In this research, a depth control system is developed with the depth estimator as a depth sensor. Only proportional-integral (PI) control will be presented, although more advanced control algorithms have shown better results at the expense of complexity (Refs. 16, 20). A discrete-time PI controller employed is given by

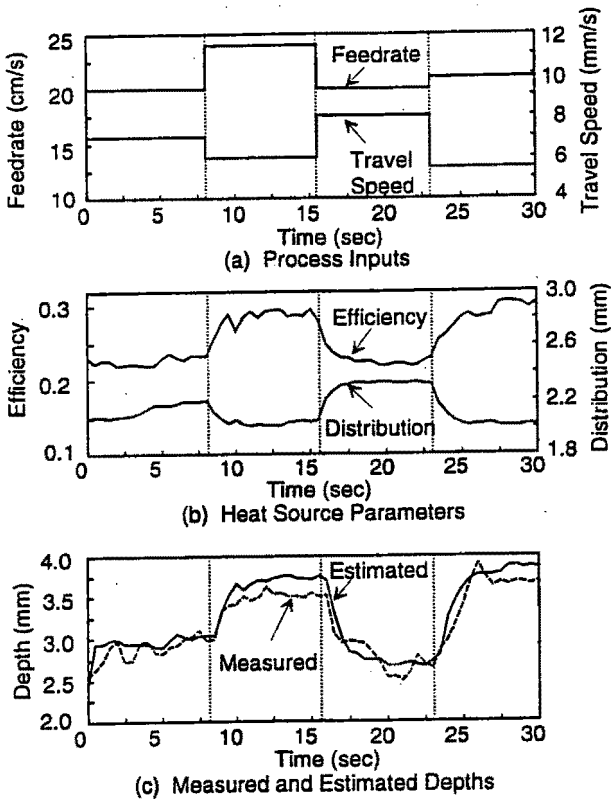


*Fig. 11 — Comparison of measured and estimated depths for time-varying welding conditions. The depth estimator provides fast depth estimates with acceptable accuracy.*

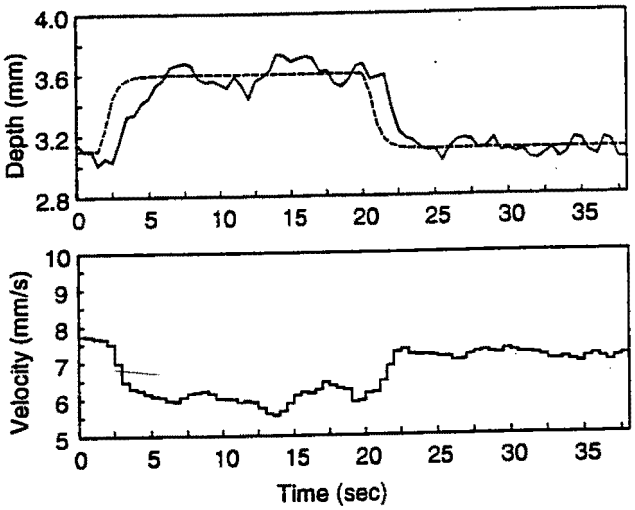


*Fig. 12 — Command following of control system (input; travel speed, output; depth, feed rate; 20 cm/s, sampling frequency; 2 Hz). The controller produces reasonably good depth output in steady-state regulation.*

$$u(z) = \left[K_P + \frac{K_I}{1 - z^{-1}}\right]\left(y^*(z) - y(z)\right) \quad (10)$$

where u(z) is the control input (either wire feed rate or travel speed), y*(z) and y(z) are the desired and actual depths, respectively, and $K_P$ and $K_I$ are the proportional and integral gains, respectively. The optimal gains for the PI controller can be determined either by simulation or by experiment.

In welding, steady-state regulation is much more important than transient tracking because the desired depth is usually a fixed value. Thus, good command following performance in response to a step change in reference command is sufficient in most situations. Figure 12 shows the command following property of the control system with travel speed as the process input. Wire feed rate is kept constant during the process. Except for some time delay immediately after a step change in the desired depth, the steady-state performance of the control system is reasonably good. Depth variation around the desired value is caused by either measurement error or process noise. Similar performance on depth regulation can be obtained by using wire feed rate as an input.

In welding, various forms of disturbances may exist (e.g., thickness change, change of material properties, parameter drifts of the welding machines, etc.). Figure 13 shows the disturbance rejection property of the control system with wire feed rate as an input using step changes in the travel speed as the disturbance. At the time t = 5 s, the travel speed increases from 6 mm/s (14.2 in./min) to 8 mm/s (18.9 in./min), thus resulting in a quick decrease in the depth output. The controller increases the feed rate to compensate for the decreased depth. A similar trend is observed in the disturbance introduced at time t = 25 s.

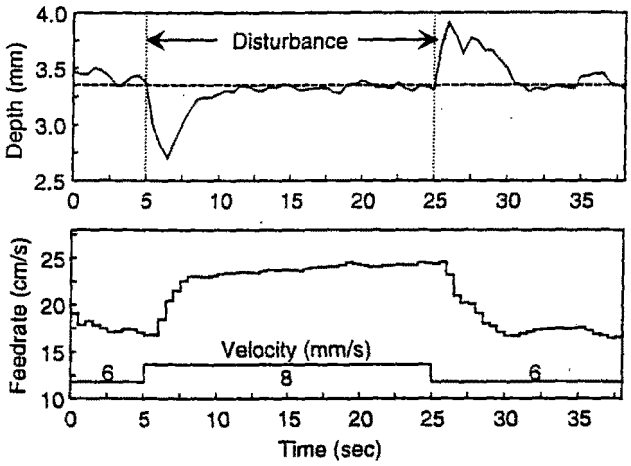


*Fig. 13 — Disturbance rejection of control system (input; feed rate, output; depth, disturbance; travel speed, sampling frequency; 2 Hz). It is noted that disturbances introduced at time t = 5 and 25 s are rejected quickly by control action.*

## Conclusions

In this paper, a method for real-time estimation of the depth of penetration in gas metal arc welding (GMAW) was proposed and tested. In an attempt to describe the finger penetration (deep and narrow penetration) observed in GMAW, a heat transfer model based on a lateral Gaussian heat source was proposed. This heat transfer model, along with a parameter identification scheme and a temperature-measurement system, comprises the real-time depth estimator that can deal with time-varying welding conditions. The depth estimator has been shown to provide accurate and fast depth estimates for real-time control.

Even though the depth estimator was proposed for application to GMAW, the same algorithm can be applied to various types of arc welding processes, such as gas tungsten arc welding (GTAW), because this method is based not on the characteristics of each arc welding process, but on the heat conduction phenomena in the solid region, which are common to all welding processes. Depending on the weld pool shape, proper heat source models, such as top Gaussian heat source shown in Fig. 3, can be used in the temperature expression instead of the lateral Gaussian heat source.

A closed-loop control system to regulate the depth has been developed using this thermally based depth estimator as a depth sensor. Both wire feed rate and travel speed were shown to have a good control power over the depth when used as a process input. The closed-loop control system produced good performance both on command following and disturbance rejection.

Throughout this research, only bead-on-plate welding has been conducted. The usage of the depth estimator presented here is limited to partial penetration welds. Application of the depth estimator to other weld profiles and fillet welds may require some modification. This is the future research topic. Another important limitation of the depth estimator is related to the thermal properties of the materials to be welded. Because the depth estimator is based on heat conduction relationship, it cannot be effectively used for the material with very low thermal diffusivity. However, the depth estimator can be used to many important metals with relatively high thermal diffusivity (e.g., low-carbon steel = 0.08 $cm^2/s$, stainless steel = 0.07 $cm^2/s$, aluminum = 0.7 $cm^2/s$).

*Acknowledgment*

This project was supported by the U.S. Department of Energy under contract number DE-FG02-85ER13331.

*References*

1. Hardt, D. E., and Katz, J. M. 1984. Ultrasonic measurement of weld penetration. *Welding Journal* 63(9): 273-s to 281-s.

2. Lott, L. A. 1984. Ultrasonic detection of molten solid interface of weld pools. *Materials Evaluation* 42: 337-341.

3. Sorenson, C. D. 1985. Digital signal processing as a diagnostic tool for GTA welding. Ph.D. thesis, Cambridge, Mass., M.I.T.

4. Tam, A. S., and Hardt, D. E. 1989. Weld pool impedance for pool geometry measurement: stationary and non-stationary pools. *ASME Journal of Dynamic Systems, Measurement, and Control* 111(4): 545-553.

5. Renwick, R. J., and Richardson, R. W. 1983. Experimental investigation of GTA weld pool oscillations. *Welding Journal* 62(2): 29-s to 35-s.

6. Zacksenhouse, M., and Hardt, D. E. 1983. Weld pool impedance identification for size measurement and control. *ASME Journal of Dynamic Systems, Measurement, and Control* 105(3): 179-184.

7. Richardson, R. W., Gutow, D. A., Anderson, R. A., and Farson, D. F. 1984. Coaxial arc weld pool viewing for process monitoring and control. *Welding Journal* 63(3): 43-50.

8. Khan, M. A., Madsen, N. H., Goodling, J. S., and Chin, B. A. 1986. Infrared thermography as a control for the welding process. *Optical Engineering* 25(6): 799-805.

9. Nomura, H., Satoh, Y., Tohno, K., Satoh, Y., and Kurotori, M. 1980. Arc light intensity controls current in SA welding system. *Welding and Metal Fabrication* 48: 457-463.

10. Bates, B. E., and Hardt, D. E. 1985. A real-time calibrated thermal model for closed-loop weld bead geometry control. *ASME Journal of Dynamic Systems, Measurement, and Control* 107(1): 25-33.

11. Somers, T. 1986. Control of GTA weld penetration based on infrared temperature measurement. M.S. thesis, Cambridge, Mass., M.I.T.

12. Rosenthal, D. 1946. The theory of moving sources of heat and its application to metal treatments. Transaction of the ASME : 849-866.

13. Eagar, T. W., and Tsai, N.-S. 1983. Temperature fields produced by traveling distributed heat sources. *Welding Journal* 62(12): 346-s to 355-s.

14. Song, J.-B., and Hardt, D. E. 1990. Estimation of weld bead depth for in-process control. *Automation of Manufacturing Processes*, ASME Winter Annual Meeting, DSC-Vol. 22: 39-45.

15. Doumanidis, C. C. 1992. Hybrid modeling for control of weld pool dimensions. *Proceedings of the Japan-U.S.A. Symposium on Flexible Automation* 1: 317-323.

16. Song, J.-B. 1992. Multivariable adaptive control in GMA welding using a thermally based depth estimator. Ph.D. thesis. Cambridge, Mass., M.I.T.

17. Myers, P. S., Uyehara, O. A., and Borman, G. L. 1967. Fundamentals of heat flow in welding. Welding Research Council Bulletin 123: 1-46.

18. Marquardt, D. W. 1963. An algorithm for least-squares estimation of nonlinear parameters. *Journal of the Society for Industrial and Applied Mathematics* 11(2): 431-441.

19. Chuang, T. H. 1991. Design of radiation pyrometer for the real-time control of weld penetration. M.S. thesis, Cambridge, Mass., M.I.T.

20. Song, J.-B., and Hardt, D. E. 1992. Simultaneous control of bead width and depth geometry in gas metal arc welding. *Proceedings of the 3rd International Conference on Trends in Welding Research*, Gatlinburg, Tenn., ASM International, Materials Park, Ohio.